Li *et al. J Mater Inf* 2023;3:25
**DOI:** 10.20517/jmi.2023.29

**Journal of Materials Informatics**

**Research Article**

**Open Access**

# Investigation of dual atom doped single-layer $MoS_2$ for electrochemical reduction of carbon dioxide by first-principle calculations and machine-learning

**Huidong Li, Chaofang Deng, Fuhua Li, Mengbo Ma, Qing Tang***

School of Chemistry and Chemical Engineering, Chongqing Key Laboratory of Theoretical and Computational Chemistry, Chongqing University, Chongqing 401331, China.

***Correspondence to:** Dr. Qing Tang, School of Chemistry and Chemical Engineering, Chongqing Key Laboratory of Theoretical and Computational Chemistry, Chongqing University, No. 55, South University City Road, Shapingba District, Chongqing 401331, China. E-mail: qingtang@cqu.edu.cn

**How to cite this article:** Li H, Deng C, Li F, Ma M, Tang Q. Investigation of dual atom doped single-layer $MoS_2$ for electrochemical reduction of carbon dioxide by first-principle calculations and machine-learning. *J Mater Inf* 2023;3:25. https://dx.doi.org/10.20517/jmi.2023.29

**Received:** 12 Jul 2023 **First Decision:** 11 Aug 2023 **Revised:** 27 Oct 2023 **Accepted:** 13 Nov 2023 **Published:** 21 Nov 2023

**Academic Editors:** Xingjun Liu, Liming Yang **Copy Editor:** Dong-Li Li **Production Editor:** Dong-Li Li

## Abstract

The exploration of efficient electrocatalysts for carbon dioxide reduction reaction ($CO_2RR$) with viable activity and superior selectivity remains a great challenge. The efficiency of $CO_2RR$ over traditional transition metal-based catalysts is restricted by their inherent scaling relationships, so breaking this scaling relationship is the key to improving the catalytic performance. In this work, inspired by the recent experimental progress in the synthesis of dual atom catalysts (DACs), we reported a rational design of novel DACs with two transition metal atoms embedded in defective $MoS_2$ with S vacancies for $CO_2$ reduction; 21 metal dimer systems were selected, including six homonuclear catalysts ($MoS_2$-$M_2$, M = Cu, Fe, Ni, Mn, Cr, Co) and 15 heteronuclear catalysts ($MoS_2$-$M_1M_2$). First-principles calculations showed that the $MoS_2$-NiCr system not only breaks the linear relationship of key intermediates but also possesses a low overpotential of 0.58 V and superior selectivity in the process of methane generation, which can be used as a promising catalyst for methane formation from $CO_2$ electroreduction. Notably, by combining random forest regression machine learning study, we found that the $CO_2RR$ activity of DACs is essentially controlled by some fundamental factors, such as the distance between metal centers and the number of outer electrons in the metal atoms. Our findings provide profound insights for the design of efficient DACs for $CO_2RR$.

**Keywords:** Electrocatalysis, $CO_2RR$, dual atom catalysts, random forest regression

## INTRODUCTION

The increasing consumption of fossil fuels has induced massive release of carbon dioxide ($CO_2$) in the atmosphere and caused severe energy crisis and environmental pollution on a global scale[1,2]. One sustainable approach is to decrease $CO_2$ emissions while transforming $CO_2$ into value-added products. Nevertheless, the $CO_2$ molecule is very stable, which requires a high activation energy to activate and break the C=O bond[3-7]. Among those developed methods[8,9], the electrochemical $CO_2$ reduction reaction ($CO_2RR$) is one promising solution and has received lots of experimental and theoretical attention owing to its simple operation, controllable selectivity, and practical potential for industrial applications[10,11].

In particular, the single-atom catalysts (SACs) have been a rapidly developing field in recent years owing to their powerful potential for heterogeneous catalysis[12]. The well-defined active sites provide a great platform for investigating the reaction mechanism and establishing the correlation between structures and activity[3,11,13-20]. Significant progress has been made in applying SACs for single-intermediate electrochemical reactions, i.e., the hydrogen evolution reaction (HER)[21-24]. The SACs also exhibit promising electrocatalytic applications in other types of multi-intermediate reactions, including oxygen reduction reactions (ORR)[25-28], $CO_2RR$[29-31], and $N_2$ reduction reactions (NRR)[32,33]. The catalytic activity of SACs, however, is usually limited to the simple electronic structure and low density of metal active sites[34]. Meanwhile, the SACs tend to form metal clusters during experimental synthesis, which causes great challenges in the usage of SACs efficiently[18,35]. Moreover, due to the presence of only one type of active site, it is difficult to break the inherent linear relationship of adsorption strength of intermediates by SACs[36-38]. The catalytic activity can be regulated by balancing the adsorption of reaction intermediates on the catalyst surface[39,40].

In this case, a promising strategy to regulate the adsorption of intermediates is via introducing a secondary metal site, as indicated by prior studies[41-43]. We have termed it as dual atom catalysts (DACs)[44]. On account of the synergetic effects of dual active sites, DACs can better maximize the catalytic potential of SACs for various multi-step reactions, leading to boosted catalytic performance[45-49]. For example, Yan *et al.* experimentally synthesized the $Pt_2$ dimer dispersed on graphene, which catalyzes the hydrolytic dehydrogenation of ammonia and boron at a reaction rate nearly 17-fold faster than that of a single Pt atom[50]. Ren *et al.* synthesized Fe-Ni DACs embedded in N-doped porous carbon as a highly efficient catalyst for $CO_2$ reduction[13]. In theory, Zhao *et al.* predicted that $Cu_2$ dimer loaded on porous $C_2N$ nanosheets has high selectivity for $CH_4$ production[51]. The Co-, Ni-, and Cu-based DACs are predicted to exhibit higher activity for $O_2$ reduction than the corresponding single-atom counterparts[45,52]. In order to obtain excellent transition metal (TM)-based DACs, an appropriate stabilizing substrate is essential, which not only offers the coordination sites for stably capturing metal atoms but also acts synergistically with the active center during the electrocatalytic process. Currently, a lot of experimental and theoretical studies focus on the N-doped carbon or graphene as the stabilizing substrate. Notably, during the synthesis of 2D nanosheets of molybdenum disulfide ($MoS_2$), inherent vacancy defects are very common and easy to form, mostly S vacancies[53-55]. Not only the single S vacancy but also the double S vacancies and clustered S vacancy line can be realized experimentally[56]. These S vacancies can be used as the anchor sites for catalytic atoms due to their high binding affinity for atoms and molecules. Experimentally, many isolated metal atoms, such as Co and Pt, have been successfully anchored at the single S vacancy of $MoS_2$[57,58]. Thus, we hypothesized that the $MoS_2$ with available double S vacancies could also be a potential substrate to anchor DACs[59].

In this work, we theoretically explored the $CO_2RR$ performance of a series of dual-metal (M: Cu, Fe, Ni, Mn, Cr, Co)-doped single-layered $MoS_2$ (denoted as $MoS_2$-$M_2$ or $MoS_2$-$M_1M_2$, Figure 1) via density functional theory (DFT) calculations. In the optimized homonuclear and heteronuclear DACs, some of the adjacent

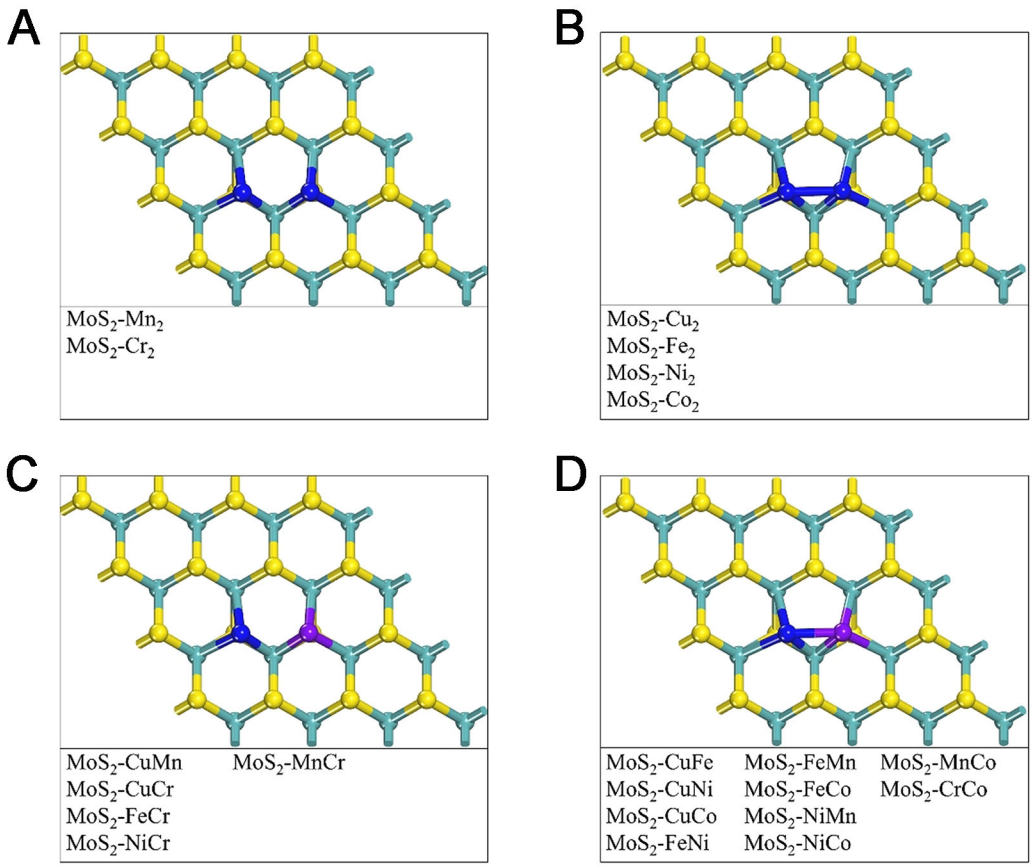


**Figure 1.** The geometric structure of $MoS_2$-$M_2$ and $MoS_2$-$M_1M_2$. Some of the adjacent metal atoms will form metal-metal bonds (B and D), while others will not (A and C). The dark cyan and yellow balls represent Mo and S atoms, respectively, and the dark blue and purple balls represent the two TM atoms. TM: Transition metal.

metal atoms will form the metal-metal bond [Figure 1B and D], while others will not [Figure 1A and C]. The results showed that water molecules would first occupy the active site, which is difficult to desorb, and would stabilize $MoS_2$-$M_2$/$M_1M_2$ for further $CO_2$ reduction. Among the examined 21 DAC compositions, $MoS_2$-NiCr is identified as a highly promising candidate for catalyzing $CO_2$ reduction to $CH_4$. More importantly, we incorporated random forest regression prediction in a machine learning approach by training the DFT calculated data to identify important feature factors that influence the activity of $CO_2$RR and the adsorption of the key *CO intermediate, where the distance between the two metal centers and the number of electrons in the outer layers of the metal atoms play a significant role.

## COMPUTATIONAL DETAILS

All the spin-unrestricted DFT calculations are performed in the DMol$^3$ code[60,61]. The exchange-correlation effect is described via the Perdew-Burke-Ernzerhof (PBE)[62] functional of the generalized gradient approximation (GGA)[63]. The double numerical plus polarization (DNP) basis is employed using the DFT semi-core pseudopotential (DSPP) for the core treatment. The van der Waals interaction between $CO_2$RR intermediates and DACs is described by empirical dispersion-corrected DFT (DFT-D3). To simulate the aqueous solvent environment, a conductor-like screening model (COSMO) is adopted[64-66]. In geometric optimization, the convergence threshold of energy is $2 \times 10^{-5}$ Ha; the maximum displacement is set as 0.005 Å, and the force applied to each atom is 0.004 Ha/Å. A 4 × 4 × 1 rectangular 2H-$MoS_2$ supercell with

adjacent double S vacancies was constructed, and a 3 × 3 × 1 Monkhorst-Pack k-mesh was used to sample the Brillouin zone. Moreover, an 18 Å vacuum space was set to avoid interactions of adjacent images. The canonical ensemble (NVT) ab initio molecular dynamics (AIMD) simulations are performed in a Nosé-Hoover thermostat at 300K for five picoseconds (ps) in a time step of one femtosecond (fs).

The formation energies of homonuclear and heteronuclear DACs, $E_f$, are calculated by the following equation[67]:

$$E_f = \frac{1}{N}\left[E_{total} - \left(E_{MoS_2} + N \times E_{TM}\right) + N \times E_{coh}\right]$$

where $N$ represents the number of doped atoms, $E_{total}$ is the total energy of DACs, $E_{MoS_2}$ denotes the energy of $MoS_2$ substrate with double S vacancies, and $E_{coh}$ is the cohesive energy of the dopant.

According to the computational hydrogen electrode (CHE) model[68], the Gibbs free energy change (ΔG) of each elementary reaction step of $CO_2$RR is calculated by ΔG = ΔE + ΔZPE - TΔS, where ΔE is the reaction energy change calculated by DFT calculations, while ΔZPE and TΔS represent the difference in zero-point and entropy change at 298 K. For gas phase molecules, the entropy is derived from the NIST database and details are provided in the Supporting Information [Supplementary Table 1].

The limiting potential ($U_L$) of the reaction is calculated as $U_L = -\Delta G_{max}/e$, where $\Delta G_{max}$ corresponds to the maximum free energy change among all the $CO_2$RR elementary steps.

## RESULTS AND DISCUSSION

### Stability

According to the above equations, we calculated the formation energy ($E_f$) [Figure 2A] to assess the thermodynamic stability of the six kinds of homonuclear DACs and 15 kinds of heteronuclear DACs. The $E_f$ of all DACs were negative, ranging from -4.92 to -6.16 eV [Supplementary Table 2], indicating high thermodynamic stability. In addition, the AIMD simulations are carried out to verify the dynamic stability of the DACs. From Figure 2B to E ($MoS_2$-MnCr, $MoS_2$-FeMn, $MoS_2$-CrCo, and $MoS_2$-NiCr), the temperature slightly fluctuates around 300 K, and the energy changes within ± 0.01 eV. No obvious deformation occurs in these frameworks during the AIMD simulation, further confirming the high dynamic stability of the catalysts.

### Activation of $CO_2$

The activation of $CO_2$ over the active center is the first step during electrocatalytic $CO_2$RR. However, from Supplementary Table 3, water adsorption is energetically more preferable than $CO_2$ except for $MoS_2$-MnCr. From the optimized structures [Supplementary Figure 1], the O atom of the adsorbed $H_2O$ is coordinated to one single metal center or the metal-metal bridge site. Note that the adsorbed water molecule cannot split spontaneously due to its highly endothermic dissociation process (0.28~1.07 eV, Supplementary Table 4). Therefore, we subsequently considered $CO_2$ adsorption and reduction after water molecules first occupy the active site. The binding interaction between $CO_2$ and $MoS_2$-embedded DACs ranges from -0.45 to -0.98 eV [Supplementary Figure 2]. Especially, the binding strength of $CO_2$ on $MoS_2$-NiCr is strong with high adsorption free energy of -0.98 eV and curved O–C–O bond angle of 139.106°, which is accompanied by considerable charge transfer of around 0.6 |e| from catalyst to $CO_2$ [Figure 3A]. Note that in the case of $MoS_2$-NiCr, the two O atoms of $CO_2$ are coordinated to the Ni and Cr centers, respectively. In other DAC systems, only one of the O atoms of $CO_2$ is coordinated to one metal center, which is accompanied by

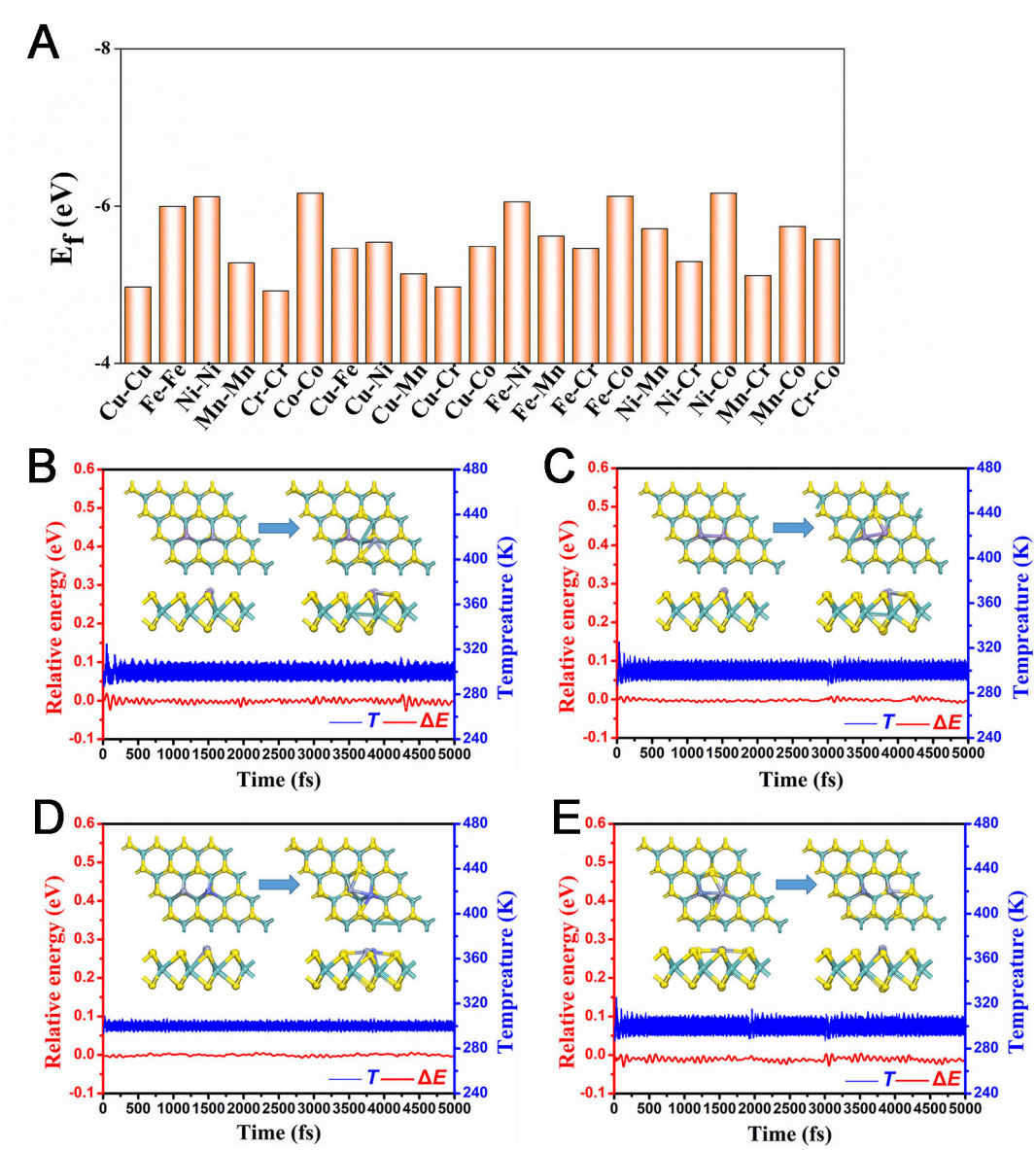


**Figure 2.** (A) The formation energy of different transition metals embedded in $MoS_2$; The energy fluctuations of (B) $MoS_2$-MnCr, (C) $MoS_2$-FeMn, (D) $MoS_2$-CrCo , and (E) $MoS_2$-NiCr in AIMD simulations for 5 ps under 300 K with a time step of 1 fs. AIMD: Ab initio molecular dynamics; fs: femtosecond.

weaker adsorption strength (-0.45~-0.88 eV) and less charge transfer (0.01~0.02 |e|) between the anchored metal dimer and $CO_2$ ($MoS_2$-CrCo is shown as an example in Figure 3B). However, the favorable adsorption proves that $CO_2$ molecules can be effectively captured and activated by the metal dimers embedded in sulfur vacancies of $MoS_2$.

## Scaling relations

In most cases, the potential limiting step for $CO_2$ electroreduction is the reduction of *COOH to *CO (two-electron reduction) or the reduction of *CO to *CHO (deep reduction). Thus, the overall catalytic efficiency depends strongly on the adsorption energies of *COOH [$E_{ads}$(COOH)], *CO [$E_{ads}$(CO)], and *CHO [$E_{ads}$(CHO)][69,70]. The reduction of $CO_2$ to CO involves a two-step electroreduction, i.e.,

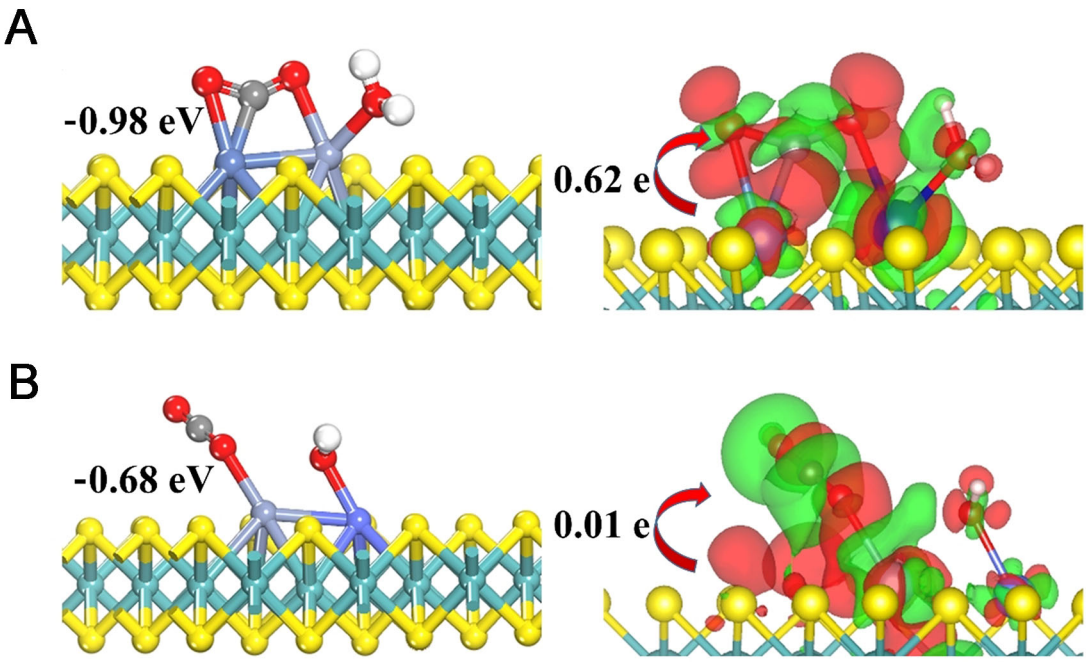


**Figure 3.** The adsorption geometry and charge density difference of $CO_2$ adsorption over (A) $MoS_2$-NiCr and (B) $MoS_2$-CrCo DACs, with an isosurface level of 0.002 e·Å$^{-3}$. The green and red regions represent electron depletion and accumulation, respectively. DACs: Dual atom catalysts.

$*CO_2 + H^+ + e^- \rightarrow *COOH$ and $*COOH + H^+ + e^- \rightarrow *CO + H_2O$, while *CO to *CHO is a hydrogenation reduction step, $*CO + H^+ + e^- \rightarrow *CHO$. The adsorption strengths of *CO and *COOH or *CHO on the conventional metal surfaces are usually linearly correlated, which limits the electrocatalytic activity[36,71]. Therefore, we first examined the adsorption of *CHO, *COOH and *CO. The detailed adsorption energy and the adsorption geometries are given in Supplementary Table 5 and Supplementary Figure 3. From Figure 4, the scaling relations are completely broken compared to those observed in pure metal surfaces. In the linear diagram of $E_{ads}$(COOH) *vs.* $E_{ads}$(CO) [Figure 4A], the scattered points are distributed in the whole region, indicating that the DAC electrocatalysts can effectively break the linear relationship. Note that most of these investigated DACs have strong *CO adsorption, which means that the generated CO would undergo further hydrogenation to form deep reduction products. For the relationship between $E_{ads}$(CO) and $E_{ads}$(CHO) [Figure 4B], the scaling relationships are slightly weakened with scattered points compared with those of the pure metal surfaces. In addition, NiCr and CrCo are two special cases that deviate greatly from the linear relationship of pure metal surfaces and show small differences between $E_{ads}$(CO) and $E_{ads}$(CHO); thus, they can be used as candidates to achieve the desired low overpotential for deep reduction products. Consequently, we selected these two systems for our subsequent calculations. We also analyzed the projected density of states (PDOS) of the NiCr and CrCo candidates after CO adsorption. From Supplementary Figure 4, within the energy region from -8 to -4 eV below the Fermi level, it can be clearly seen that the *p* orbital of C in the adsorbed *CO is strongly hybridized with the *d* orbital of the metal, proving that *CO has strong adsorption with the metal active site, which is beneficial to the deep reduction reaction of CO[72].

### The pathway of $CO_2$RR

In the following, we systematically investigated the reduction pathway of $CO_2$RR on $MoS_2$-NiCr and $MoS_2$-CrCo after the formation of strongly bound *CO (*CO is firstly produced through the two-electron

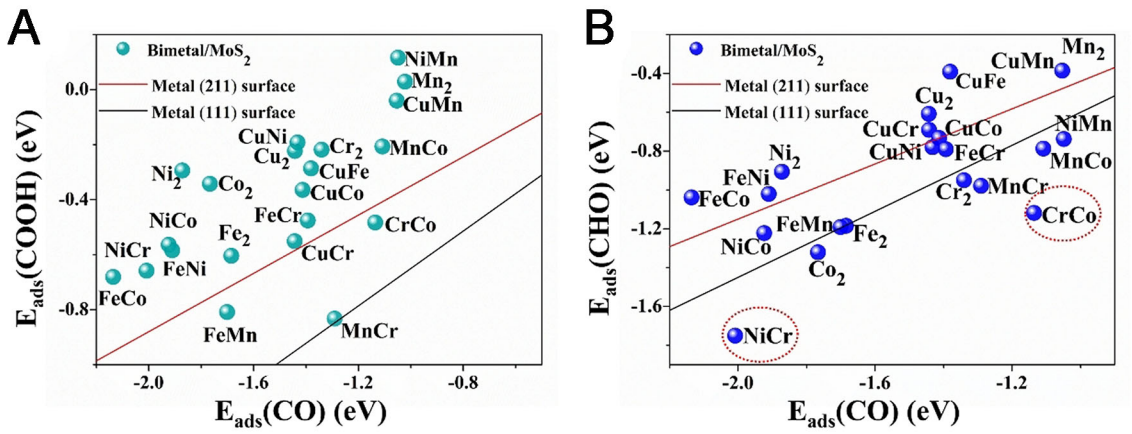


**Figure 4.** Relationship between the binding energies (A) $E_{ads}$(COOH) *vs.* $E_{ads}$(CO) and (B) $E_{ads}$(CHO) *vs.* $E_{ads}$(CO) of $MoS_2$ embedded DACs and the transition metal surfaces. The linear proportional relationships between the adsorbents were obtained on Ni, Cu, Ag, Pd, Au, Pt, and Rh surfaces[70]. DACs: Dual atom catalysts.

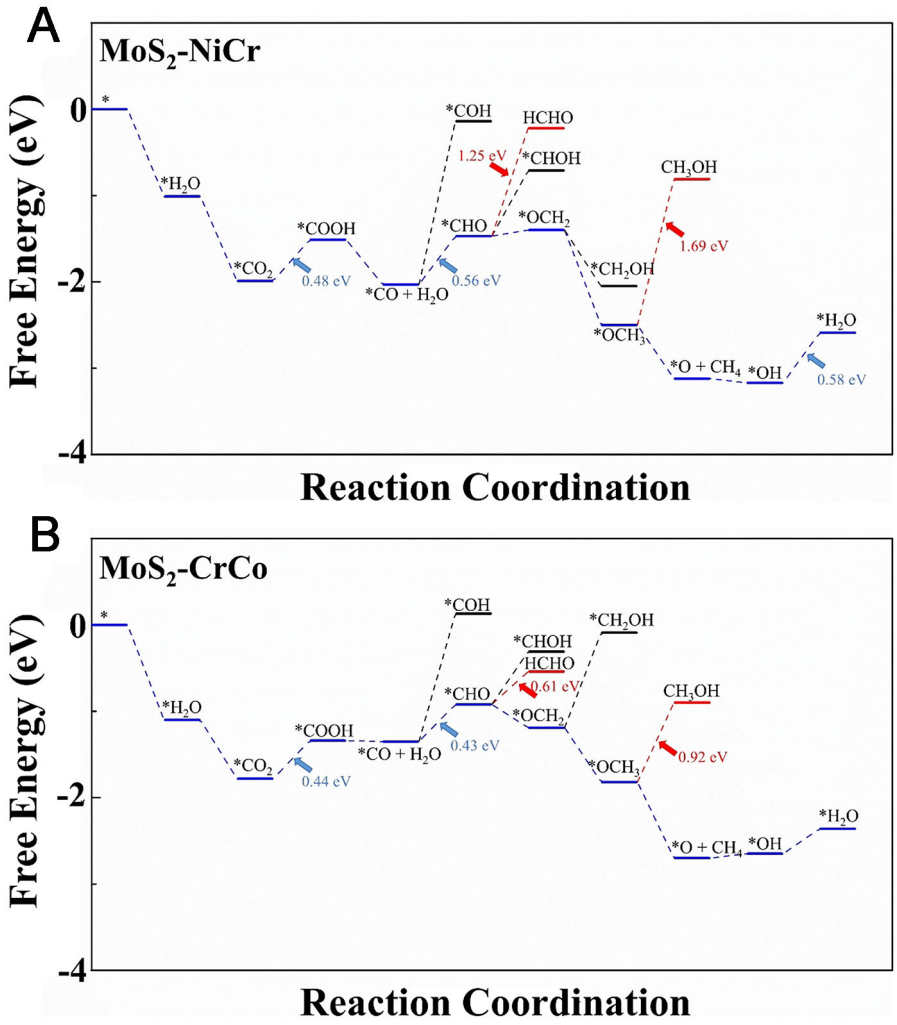


**Figure 5.** Free energy diagrams of the electroreduction of $CO_2$ on (A) $MoS_2$-NiCr and (B) $MoS_2$-CrCo at $U_{RHE}$ = 0 eV.

pathway: $CO_2$ → *COOH → CO). The *CO can be further reduced to other C1 products, such as HCHO, $CH_3OH$, and $CH_4$. The free energy diagrams of all the possible C1 products are shown in Figure 5, the structural schematics are shown in Supplementary Figure 5, and the detailed data of free energy are provided in Supplementary Table 6. One can see that the hydrogenation of *CO to *CHO is energetically more favorable than the formation of *COH. Moreover, for both $MoS_2$-NiCr and $MoS_2$-CrCo, the generation of $CH_4$ needs lower energy input than the generation of HCHO and $CH_3OH$, indicating that $CH_4$ would be the main reduction product of $CO_2$RR. From Figure 5A, the potential limiting step of $CH_4$ formation on $MoS_2$-NiCr corresponds to *CO reduction to *CHO and *OH reduction to $H_2O$, which need comparable endothermic free energy of 0.56 and 0.58 eV, respectively. While on $MoS_2$-CrCo [Figure 5B], the potential limiting step of $CH_4$ formation corresponds to *$CO_2$ reduction to *COOH or *CO reduction to *CHO, which needs comparable endothermic free energy of 0.44 and 0.43 eV, respectively. Figure 6 shows the detailed geometry of reaction intermediates during $CH_4$ formation on $MoS_2$-NiCr and $MoS_2$-CrCo catalysts. On $MoS_2$-NiCr [Figure 6A], the various intermediates (*CHO, *$CH_2O$, *$CH_3O$, *O, and *OH) from a deep reduction of *CO are all coordinated to both the Ni and Cr atoms. In the case of $MoS_2$-CrCo [Figure 6B], the reaction intermediates are mainly singly coordinated to the Cr atom. This indicates that the Ni and Cr centers in $MoS_2$-NiCr work synergistically as dual active sites to affect the adsorption and bonding of $CO_2$RR intermediates, while in $MoS_2$-CrCo, only the Cr center plays the key role and functions as the single active site for $CO_2$RR.

### Selectivity of $CO_2$RR *vs.* HER

In $CO_2$RR, the HER always competes with $CO_2$ reduction in an aqueous solution[73]. Firstly, the occupation of sites was initially considered, and as shown in Supplementary Table 7, H adsorption in most dual-atom systems is not as strong as $H_2O$ and $CO_2$ adsorption. Therefore, the diatomic sites are more likely to take the $CO_2$RR path. Secondly, it is necessary to assess the selectivity of $CO_2$RR by comparing its limiting potential ($U_L$). In the $CO_2$ reduction process, we consider the comparison between the limiting potential of the electrochemical steps and that of HER. Accordingly, a more positive value of $\Delta U_L$ [$U_L(CO_2RR)$ - $U_L(HER)$] implies higher reaction selectivity for $CO_2$ reduction. From Figure 7, the $\Delta U_L$ of the NiCr dimer (0.26 V) is located in the upper right corner, indicating its high $CO_2$RR selectivity, while the $\Delta U_L$ of the CrCo dimer is close to 0, indicating its poor selectivity. Furthermore, the ideal electrocatalysts should be well accompanied by effective $CO_2$ activation. In other words, the strong adsorption of $CO_2$ over the catalyst can inhibit H on the catalyst surface, thus hindering the competitive HER as the $CO_2$ will occupy the available active sites[6,74,75]. The calculated adsorption free energies of *H on $MoS_2$-NiCr and $MoS_2$-CrCo metal sites are -0.84 and -0.45 eV, respectively (inset in Figure 7), while the adsorption free energies of $CO_2$ are -0.98 and -0.68 eV, respectively. This indicates that $CO_2$ adsorption is more favorable than H* adsorption. Hence, the adsorption of $CO_2$ is preferred, while the adsorption of *H is hindered. By comparing the reaction activity and selectivity, the $MoS_2$-NiCr is screened to be a promising dual-site electrocatalyst to promote the $CH_4$ formation with moderate rate-determining step (RDS) barriers and high $CO_2$RR selectivity over HER. Our theoretical prediction will provide useful insights for future experimental verification of the high electrocatalytic performance of Ni-Cr DACs supported on $MoS_2$ substrates.

### Machine learning analysis

From the data calculated above, the $CO_2$RR activity of DACs and the binding strength of the intermediate *CO are closely related, with weak CO binding favoring CO gas desorption and strong CO binding facilitating adsorption of added H to *CHO. At present, the underlying factors affecting $CO_2$RR activity remain to be discovered. Furthermore, DAC systems are much more complex than TM surfaces. Therefore, it is difficult to accurately describe the $CO_2$RR activity of DACs with only one descriptor. Without performing intensive DFT calculations, there is a strong need to identify more readily available variables to describe the $CO_2$RR activity of DACs.

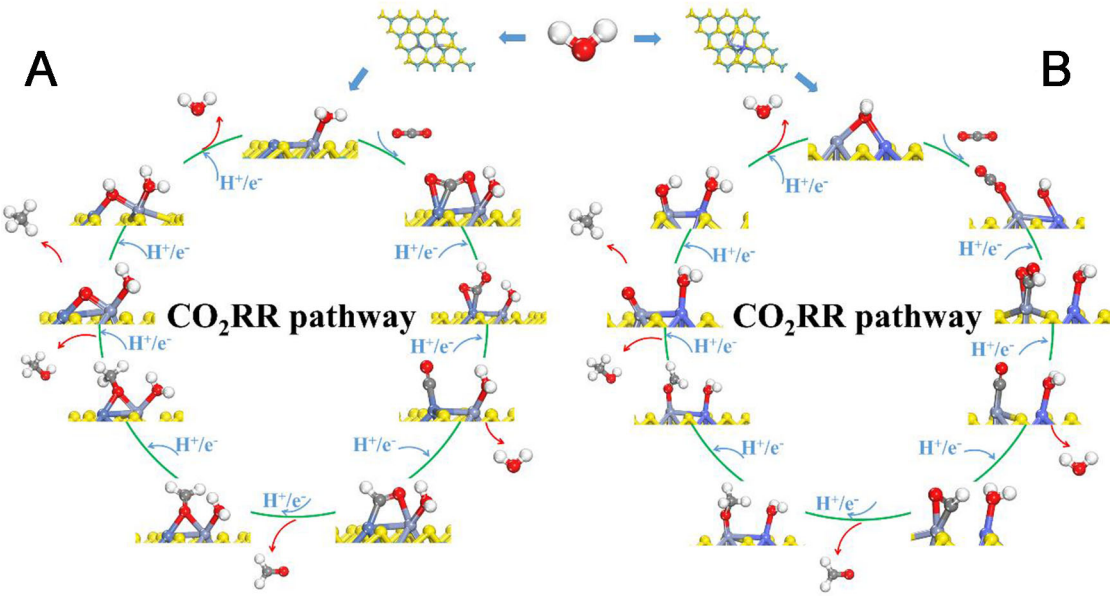


**Figure 6.** Schematics of the reaction pathway of $CH_4$ formation on (A) $MoS_2$-NiCr and (B) $MoS_2$-CrCo catalysts. $CO_2RR$: Carbon dioxide reduction reaction.

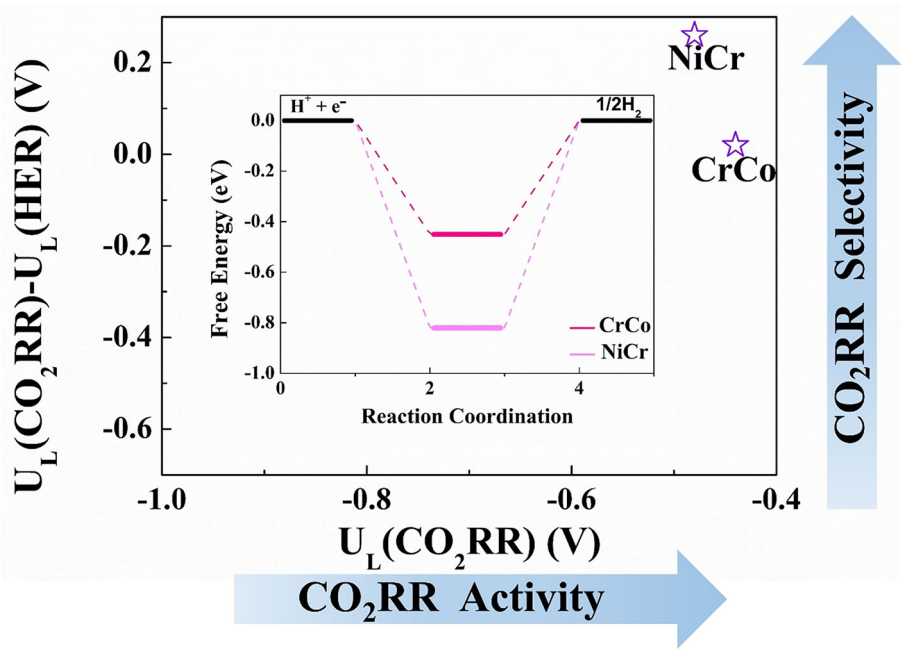


**Figure 7.** The limiting potential difference between $CO_2$ reduction [$U_L(CO_2RR)$] and HER [$U_L(HER)$] over $MoS_2$-NiCr and $MoS_2$-CrCo catalysts. The inset in the figure is the free energy diagram of HER. $CO_2RR$: Carbon dioxide reduction reaction; HER: hydrogen evolution reaction; $U_L$: limiting potential.

Thus, by using a machine learning approach, we investigated the correlation between $\Delta G_{*CO}$ or $U_L(CO)$ and the intrinsic factors of six homonuclear and 15 heteronuclear catalysts. Proper feature selection is essential for machine learning models to identify the hidden rules behind the input data. In our work, we considered seven very basic parameters to describe the geometric and electronic properties of DACs, including the

distance between two metal atoms ($d_{M-M}$), the average distance between two metal atoms and six Mo atoms ($d_{M-Mo}$), the radii of two metal atoms ($R_1$ and $R_2$), the number of outer electrons of two metal atoms ($Ne_1$ and $Ne_2$), the Pauling electronegativity ($P_1$ and $P_2$), the first ionization energy ($I_1$ and $I_2$), and the electron affinity ($A_1$ and $A_2$). Importantly, we examined the correlations between the factors, and as can be seen in Supplementary Figure 6, most combinations of factors are poorly related to each other. Some of the factors vary with the regularity of the periodic table, e.g., Ne, R, *etc*. Thus, these factors and coefficients are variables that can be approximated as independent of each other. It is important to note that we augmented the data for all the DACs studied because $MoS_2$-$M_1M_2$ and $MoS_2$-$M_2M_1$ correspond to two different sets of variable combinations [Supplementary Table 8]. In this way, each DAC possesses two sets of input features.

We used a random forest regression algorithm from the scikit-learn toolkit[76]. The DFT computed $\Delta G_{*CO}$ values were then compared with the values predicted based on the random forest study. The DFT-computed $\Delta G_{*CO}$ input data were randomly perturbed and divided into a training set and a test set in a ratio of 6:1. As shown in Figure 8A, the predicted values based on the random forest have a similar trend to the values calculated by DFT, with a lower mean square error of 0.058. There is a high $R^2$ value, 0.93 for the training score and 0.91 for the test score, indicating that the random forest prediction algorithm adequately trained the model by learning the factors inherent in the model to reach an accurate prediction. The importance of the seven features on $\Delta G_{*CO}$ was also evaluated. In Figure 8B, the distance between the metals ($d_{M-M}$) is the most influential on $\Delta G_{*CO}$, with a feature importance value of 0.34, while the sum of feature importance values of the radius of the metal atoms ($R_1$ and $R_2$) and the distance between the metal and the Mo atoms ($d_{M-Mo}$) is only 0.01. That means that the synergistic effect between the DACs has a strong influence on the catalytic efficiency. In addition, the outer electron number (Ne) of the metal atom also plays an important role, with a sum of feature importance ($Ne_1$ + $Ne_2$) of 0.20, which can be interpreted as forming a metal-metal bond between DACs that cannot efficiently bind the $CO_2$RR intermediates. However, the importance of the remaining three features (P, I, and A) was relatively insignificant. We also predicted the limiting potential in the $CO_2 \rightarrow CO$ process based on the Random Forest algorithm, and the predictions were highly similar to the DFT [Figure 8C and D]. The feature importance pie charts show similarities to those described above. Machine learning links the correlations between the intrinsic structure and the properties, providing powerful insights into the understanding of the $CO_2$RR activity of DACs. Particularly, since the activity of the dual-atom catalyst in the $CO_2$RR process is closely correlated with these important factors, we can apply these descriptors to predict the activity of other dual-atom compositions.

### Potential limitations

There is one thing that needs to be added: our work is based on first-principles calculations to investigate the activity of electrochemical reduction of $CO_2$ by dual atom doped single-layer $MoS_2$. From a theoretical point of view, the DACs predicted by us have relatively negative formation energies ($E_f$) and stable structures through AIMD, which indicates that it is feasible to synthesize such structures. Recently, an ingenious approach has successfully assembled DACs of Ni and Fe into the interlayer of $MoS_2$[77]. These DACs exhibit higher catalytic activity toward acidic water splitting. Our predicted $MoS_2$-FeNi structure was confirmed through this experiment. Therefore, these structures that we predict, namely the doping of different dual atoms (Cu, Co, Cr, Mn, *etc*.) in the single-layer $MoS_2$, are expected to be realized in the future.

Furthermore, our computations rely on a traditional CHE model that neglects the display potential and display solvation factors, which do affect the precision of the performance evaluation to some extent. Although the method has some limitations in the evaluation of activity due to the significant computational cost savings and relatively accurate simulation accuracy of the CHE model, this method is very popular for large-scale prediction and performance screening of new materials[78-83]. In other words, while taking into account the calculation speed and accuracy, the performance evaluation at the same atomic level is also of great reference significance.

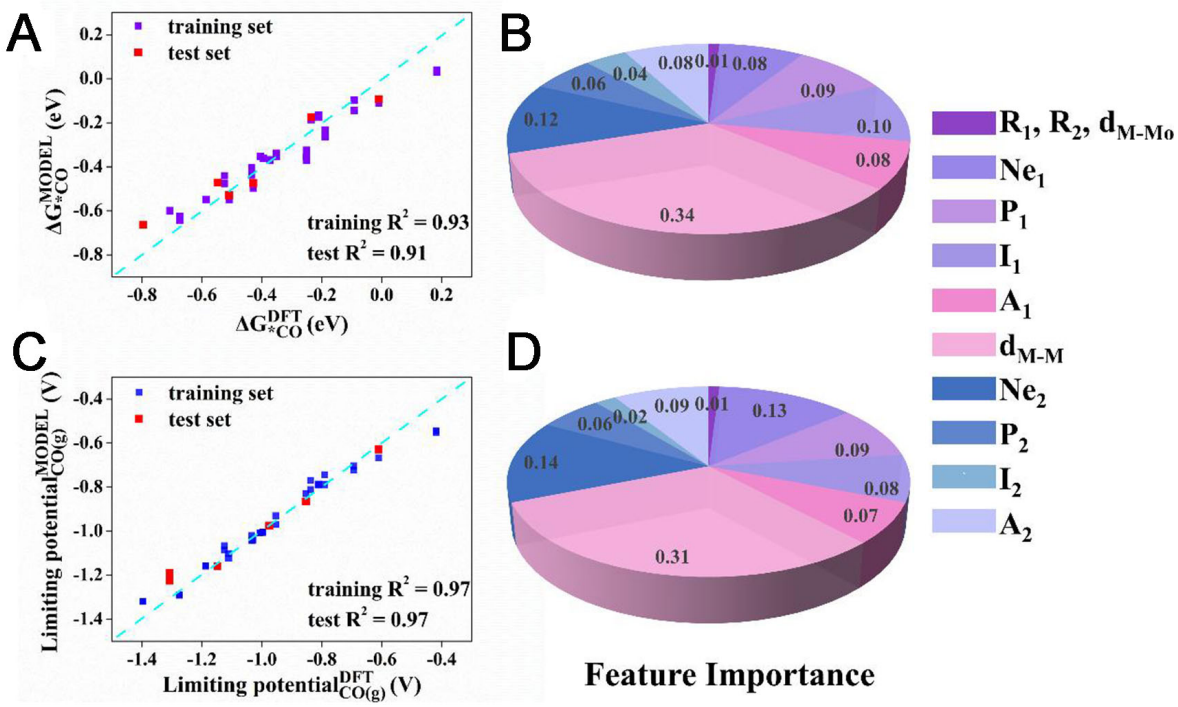


**Figure 8.** Comparison of (A) $\Delta G_{*CO}$ and (C) [$U_L$(CO)] obtained by DFT with values predicted by machine learning; (B and D) feature importance based on a random forest regression. DFT: Density functional theory.

## CONCLUSION

In summary, the reaction activity of various dual atoms embedded in defective $MoS_2$ monolayers, named $MoS_2$-$M_2$/M1M2, for $CO_2$ reduction was systematically studied using computational DFT approaches. We theoretically studied 21 dimer electrocatalysts. Our results demonstrate that the defective $MoS_2$ monolayer with double S vacancies can anchor the two TM atoms stably. Through the analysis of the adsorption relationship of key intermediates, it was found that $MoS_2$-CrCo and $MoS_2$-NiCr candidates significantly deviated from the linear relationship; thus, they were selected for further analysis of deep reduction. We found that $MoS_2$-CrCo shows a lower barrier energy for $CH_4$ production (0.44 eV), but its selectivity ($\Delta U_L$ = 0.02 eV) over competitive HER is low. In contrast, the $MoS_2$-NiCr system possesses superior selectivity ($\Delta U_L$ = 0.26 eV) and catalytic activity for $CH_4$ production with a low rate-determining electrochemical barrier of 0.58 V. In the whole reaction process, water exists in the form of coordination in the formation process of C1 products. Moreover, our machine learning study demonstrated that adsorption of the key *CO intermediate and $CO_2$RR activity can be well described by some basic parameters, such as the distance between the center of metal atoms and the number of outer electrons of the metal atoms. This work presents an atomic-level investigation of the screening and design of novel DACs supported on defective $MoS_2$, providing useful insights for further investigations, including theoretical and experimental attempts.

## DECLARATIONS

### Acknowledgments

We acknowledged the support provided by the National Natural Science Foundation of China (No.21903008) and the Chongqing Science and Technology Commission (cstc2020jcyj-msxmX0382). This research used resources from the National Supercomputer Center in Guangzhou.

### Authors' contributions

Conceived the idea for scientific research: Tang Q
Developed the theoretical models and performed the theoretical calculations: Li H
Assisted in processing the data of DFT calculations: Li H, Ma M
Provided technical support for machine learning and completed analysis and processing of data: Deng C
Wrote the manuscript and finalized it with support: Li H, Deng C, Li F, Ma M, Tang Q

### Availability of data and materials

Not applicable.

### Financial support and sponsorship

The authors would like to thank the support provided by the National Natural Science Foundation of China (No.21903008) and the Chongqing Science and Technology Commission (cstc2020jcyj-msxmX0382).

### Conflicts of interest

All authors declared that there are no conflicts of interest.

### Ethical approval and consent to participate

Not applicable.

### Consent for publication

Not applicable.



## REFERENCES

1. Goeppert A, Czaun M, Surya Prakash GK, Olah GA. Air as the renewable carbon source of the future: an overview of $CO_2$ capture from the atmosphere. *Energy Environ Sci* 2012;5:7833-53. DOI
2. Ding M, Flaig RW, Jiang HL, Yaghi OM. Carbon capture and conversion using metal-organic frameworks and MOF-based materials. *Chem Soc Rev* 2019;48:2783-828. DOI PubMed
3. Zhu DD, Liu JL, Qiao SZ. Recent advances in inorganic heterogeneous electrocatalysts for reduction of carbon dioxide. *Adv Mater* 2016;28:3423-52. DOI PubMed
4. Fan Q, Hou P, Choi C, et al. Activation of Ni particles into single Ni–N atoms for efficient electrochemical reduction of $CO_2$. *Adv Energy Mater* 2020;10:1903068. DOI
5. Yue Y, Sun Y, Tang C, et al. Ranking the relative $CO_2$ electrochemical reduction activity in carbon materials. *Carbon* 2019;154:108-14. DOI
6. Ling C, Li Q, Du A, Wang J. Computation-aided design of single-atom catalysts for one-pot $CO_2$ capture, activation, and conversion. *ACS Appl Mater Interfaces* 2018;10:36866-72. DOI PubMed
7. Zhang X, Wu Z, Zhang X, et al. Highly selective and active $CO_2$ reduction electrocatalysts based on cobalt phthalocyanine/carbon nanotube hybrid structures. *Nat Commun* 2017;8:14675. DOI PubMed PMC
8. Low J, Cheng B, Yu J. Surface modification and enhanced photocatalytic $CO_2$ reduction performance of $TiO_2$: a review. *Appl Surf Sci* 2017;392:658-86. DOI
9. Wang D, Huang R, Liu W, Sun D, Li Z. Fe-based MOFs for photocatalytic $CO_2$ reduction: role of coordination unsaturated sites and dual excitation pathways. *ACS Catal* 2014;4:4254-60. DOI
10. Jin S, Hao Z, Zhang K, Yan Z, Chen J. Advances and challenges for the electrochemical reduction of $CO_2$ to CO: from fundamentals to industrialization. *Angew Chem Int Ed Engl* 2021;60:20627. DOI
11. Zheng T, Jiang K, Wang H. Recent advances in electrochemical $CO_2$-to-CO conversion on heterogeneous catalysts. *Adv Mater* 2018;30:1802066. DOI PubMed
12. Zhou H, Zou X, Wu X, Yang X, Li J. Coordination engineering in cobalt-nitrogen-functionalized materials for $CO_2$ reduction. *J Phys Chem Lett* 2019;10:6551-7. DOI PubMed
13. Ren W, Tan X, Yang W, et al. Isolated diatomic Ni-Fe metal-nitrogen sites for synergistic electroreduction of $CO_2$. *Angew Chem Int Ed Engl* 2019;58:6972-6. DOI PubMed

14. Li H, Wang L, Dai Y, et al. Synergetic interaction between neighbouring platinum monomers in $CO_2$ hydrogenation. *Nat Nanotechnol* 2018;13:411-7. DOI
15. Liang Z, Qu C, Xia D, Zou R, Xu Q. Atomically dispersed metal sites in MOF-based materials for electrocatalytic and photocatalytic energy conversion. *Angew Chem Int Ed Engl* 2018;57:9604-33. DOI PubMed
16. Yuan CZ, Zhan LY, Liu SJ, et al. Semi-sacrificial template synthesis of single-atom Ni sites supported on hollow carbon nanospheres for efficient and stable electrochemical $CO_2$ reduction. *Inorg Chem Front* 2020;7:1719-25. DOI
17. Han L, Song S, Liu M, et al. Stable and efficient single-atom Zn catalyst for $CO_2$ reduction to $CH_4$. *J Am Chem Soc* 2020;142:12563-7. DOI
18. Yang XF, Wang A, Qiao B, Li J, Liu J, Zhang T. Single-atom catalysts: a new frontier in heterogeneous catalysis. *Acc Chem Res* 2013;46:1740-8. DOI PubMed
19. Chen Y, Ji S, Chen C, Peng Q, Wang D, Li Y. Single-atom catalysts: synthetic strategies and electrochemical applications. *Joule* 2018;2:1242-64. DOI
20. Wang Y, Mao J, Meng X, Yu L, Deng D, Bao X. Catalysis with two-dimensional materials confining single atoms: concept, design, and applications. *Chem Rev* 2019;119:1806-54. DOI PubMed
21. Chen W, Pei J, He CT, et al. Rational design of single molybdenum atoms anchored on N-doped carbon for effective hydrogen evolution reaction. *Angew Chem Int Ed Engl* 2017;129:16302-6. DOI PubMed
22. Zhang H, An P, Zhou W, et al. Dynamic traction of lattice-confined platinum atoms into mesoporous carbon matrix for hydrogen evolution reaction. *Sci Adv* 2018;4:eaao6657. DOI PubMed PMC
23. Fei H, Dong J, Arellano-Jiménez MJ, et al. Atomic cobalt on nitrogen-doped graphene for hydrogen generation. *Nat Commun* 2015;6:8668. DOI PubMed PMC
24. Luo Z, Ouyang Y, Zhang H, et al. Chemically activating $MoS_2$ via spontaneous atomic palladium interfacial doping towards efficient hydrogen evolution. *Nat Commun* 2018;9:2120. DOI PubMed PMC
25. Tian S, Deng C, Tang Y, Tang Q. Effect of adatom doping on the electrochemical performance of 1T'-$MoS_2$ for oxygen reduction reactions. *J Phys Chem C* 2020;124:24899-907. DOI
26. Tian S, Tang Q. Activating transition metal dichalcogenide monolayers as efficient electrocatalysts for the oxygen reduction reaction *via* single atom doping. *J Mater Chem C* 2021;9:6040-50. DOI
27. Chen Y, Tian S, Tang Q. First-principles studies on electrocatalytic activity of novel two-dimensional $MA_2Z_4$ monolayers toward oxygen reduction reaction. *J Phys Chem C* 2021;125:22581-90. DOI
28. Han Y, Wang YG, Chen W, et al. Hollow N-doped carbon spheres with isolated cobalt single atomic sites: superior electrocatalysts for oxygen reduction. *J Am Chem Soc* 2017;139:17269-72. DOI PubMed
29. Yang HB, Hung SF, Liu S, et al. Atomically dispersed Ni(I) as the active site for electrochemical $CO_2$ reduction. *Nat Energy* 2018;3:140-7. DOI
30. Ma M, Li F, Tang Q. Coordination environment engineering on nickel single-atom catalysts for $CO_2$ electroreduction. *Nanoscale* 2021;13:19133-43. DOI PubMed
31. Raciti D, Wang C. Recent advances in $CO_2$ reduction electrocatalysis on copper. *ACS Energy Lett* 2018;3:1545-56. DOI
32. Qing G, Ghazfar R, Jackowski ST, et al. Recent advances and challenges of electrocatalytic $N_2$ reduction to ammonia. *Chem Rev* 2020;120:5437-516. DOI PubMed
33. Wu T, Zhu X, Xing Z, et al. Greatly improving electrochemical $N_2$ reduction over $TiO_2$ nanoparticles by iron doping. *Angew Chem Int Ed Engl* 2019;58:18449-53. DOI PubMed
34. Liu L, Corma A. Metal catalysts for heterogeneous catalysis: from single atoms to nanoclusters and nanoparticles. *Chem Rev* 2018;118:4981-5079. DOI PubMed PMC
35. Liu JC, Xiao H, Li J. Constructing high-loading single-atom/cluster catalysts via an electrochemical potential window strategy. *J Am Chem Soc* 2020;142:3375-83. DOI PubMed
36. Hansen HA, Varley JB, Peterson AA, Nørskov JK. Understanding trends in the electrocatalytic activity of metals and enzymes for $CO_2$ reduction to CO. *J Phys Chem Lett* 2013;4:388-92. DOI PubMed
37. Calle-Vallejo F, Loffreda D, Koper MT, Sautet P. Introducing structural sensitivity into adsorption-energy scaling relations by means of coordination numbers. *Nat Chem* 2015;7:403-10. DOI PubMed
38. Abild-Pedersen F, Greeley J, Studt F, et al. Scaling properties of adsorption energies for hydrogen-containing molecules on transition-metal surfaces. *Phys Rev Lett* 2007;99:016105. DOI
39. Nørskov JK, Bligaard T, Rossmeisl J, Christensen CH. Towards the computational design of solid catalysts. *Nat Chem* 2009;1:37-46. DOI PubMed
40. Man IC, Su HY, Calle-Vallejo F, et al. Universality in oxygen evolution electrocatalysis on oxide surfaces. *ChemCatChem* 2011;3:1159-65. DOI
41. Yang Y, Qian Y, Li H, et al. O-coordinated W-Mo dual-atom catalyst for pH-universal electrocatalytic hydrogen evolution. *Sci Adv* 2020;6:eaba6586. DOI PubMed PMC
42. Guo X, Gu J, Lin S, Zhang S, Chen Z, Huang S. Tackling the activity and selectivity challenges of electrocatalysts toward the nitrogen reduction reaction via atomically dispersed biatom catalysts. *J Am Chem Soc* 2020;142:5709-21. DOI PubMed
43. Deng C, Su Y, Li F, Shen W, Chen Z, Tang Q. Understanding activity origin for the oxygen reduction reaction on bi-atom catalysts by DFT studies and machine-learning. *J Mater Chem A* 2020;8:24563-71. DOI

44. Lv X, Wei W, Huang B, Dai Y, Frauenheim T. High-throughput screening of synergistic transition metal dual-atom catalysts for efficient nitrogen fixation. *Nano Lett* 2021;21:1871-8. DOI PubMed
45. Li X, Zhong W, Cui P, Li J, Jiang J. Design of efficient catalysts with double transition metal atoms on $C_2N$ layer. *J Phys Chem Lett* 2016;7:1750-5. DOI PubMed
46. Jiao J, Lin R, Liu S, et al. Copper atom-pair catalyst anchored on alloy nanowires for selective and efficient electrochemical reduction of $CO_2$. *Nat Chem* 2019;11:222-8. DOI PubMed
47. Cao N, Chen Z, Zang K, et al. Doping strain induced bi-$Ti^{3+}$ pairs for efficient $N^2$ activation and electrocatalytic fixation. *Nat Commun* 2019;10:2877. DOI PubMed PMC
48. Li X, Sun Y, Xu J, et al. Selective visible-light-driven photocatalytic $CO_2$ reduction to $CH_4$ mediated by atomically thin $CuIn_5S_8$ layers. *Nat Energy* 2019;4:690-9. DOI
49. Fu J, Dong J, Si R, et al. Synergistic effects for enhanced catalysis in a dual single-atom catalyst. *ACS Catal* 2021;11:1952-61. DOI
50. Yan H, Lin Y, Wu H, et al. Bottom-up precise synthesis of stable platinum dimers on graphene. *Nat Commun* 2017;8:1070. DOI PubMed PMC
51. Zhao J, Zhao J, Li F, Chen Z. Copper dimer supported on a $C_2N$ layer as an efficient electrocatalyst for $CO_2$ reduction reaction: a computational study. *J Phys Chem C* 2018;122:19712-21. DOI
52. Hunter MA, Fischer JMTA, Yuan Q, Hankel M, Searles DJ. Evaluating the catalytic efficiency of paired, single-atom catalysts for the oxygen reduction reaction. *ACS Catal* 2019;9:7660-7. DOI
53. Chen X, Berner NC, Backes C, Duesberg GS, Mcdonald AR. Functionalization of two-dimensional $MoS_2$: on the reaction between $MoS_2$ and organic thiols. *Angewandte Chemie* 2016;128:5897-902. DOI PubMed
54. Kim IS, Sangwan VK, Jariwala D, et al. Influence of stoichiometry on the optical and electrical properties of chemical vapor deposition derived $MoS_2$. *ACS Nano* 2014;8:10551-8. DOI PubMed PMC
55. Tsai C, Li H, Park S, et al. Electrochemical generation of sulfur vacancies in the basal plane of $MoS_2$ for hydrogen evolution. *Nat Commun* 2017;8:15113. DOI PubMed PMC
56. Patra TK, Zhang F, Schulman DS, et al. Defect dynamics in 2-D $MoS_2$ probed by using machine learning, atomistic simulations, and high-resolution microscopy. *ACS Nano* 2018;12:8006-16. DOI PubMed
57. Liu G, Robertson AW, Li MM, et al. $MoS_2$ monolayer catalyst doped with isolated Co atoms for the hydrodeoxygenation reaction. *Nat Chem* 2017;9:810-6. DOI
58. Li H, Wang S, Sawada H, et al. Atomic structure and dynamics of single platinum atom interactions with monolayer $MoS_2$. *ACS Nano* 2017;11:3392-403. DOI PubMed
59. Li F, Tang Q. A di-boron pair doped $MoS_2$ (B2@$MoS_2$) single-layer shows superior catalytic performance for electrochemical nitrogen activation and reduction. *Nanoscale* 2019;11:18769-78. DOI
60. Delley B. An all-electron numerical method for solving the local density functional for polyatomic molecules. *J Chem Phys* 1990;92:508-17. DOI
61. Delley B. From molecules to solids with the $DMol^3$ approach. *J Chem Phys* 2000;113:7756-64. DOI
62. Ernzerhof M, Scuseria GE. Assessment of the Perdew-Burke-Ernzerhof exchange-correlation functional. *J Chem Phys* 1999;110:5029-36. DOI
63. Perdew JP, Burke K, Ernzerhof M. Generalized gradient approximation made simple. *Phys Rev Lett* 1996;77:3865-8. DOI PubMed
64. Keith JA, Jerkiewicz G, Jacob T. Theoretical investigations of the oxygen reduction reaction on Pt(111). *Chemphyschem* 2010;11:2779-94. DOI PubMed
65. Zhang P, Xiao BB, Hou XL, Zhu YF, Jiang Q. Layered SiC sheets: a potential catalyst for oxygen reduction reaction. *Sci Rep* 2014;4:3821. DOI PubMed PMC
66. Klamt A. Conductor-like screening model for real solvents: a new approach to the quantitative calculation of solvation phenomena. *J Phys Chem* 1995;99:2224-35. DOI
67. Verma AM, Honkala K, Melander MM. Computational screening of doped graphene electrodes for alkaline $CO_2$ reduction. *Front Energy Res* 2021;8:606742. DOI
68. Nørskov JK, Rossmeisl J, Logadottir A, et al. Origin of the overpotential for oxygen reduction at a fuel-cell cathode. *J Phys Chem B* 2004;108:17886-92. DOI
69. Peterson AA, Nørskov JK. Activity descriptors for $CO_2$ electroreduction to methane on transition-metal catalysts. *J Phys Chem Lett* 2012;3:251-8. DOI
70. Shi C, Hansen HA, Lausche AC, Nørskov JK. Trends in electrochemical $CO_2$ reduction activity for open and close-packed metal surfaces. *Phys Chem Chem Phys* 2014;16:4720-7. DOI PubMed
71. Ouyang Y, Shi L, Bai X, Li Q, Wang J. Breaking scaling relations for efficient $CO_2$ electrochemical reduction through dual-atom catalysts. *Chem Sci* 2020;11:1807-13. DOI PubMed PMC
72. Wang S, Li L, Li J, et al. High-throughput screening of nitrogen-coordinated bimetal catalysts for multielectron reduction of $CO_2$ to $CH_4$ with high selectivity and low limiting potential. *J Phys Chem C* 2021;125:7155-65. DOI
73. Zhang YJ, Sethuraman V, Michalsky R, Peterson AA. Competition between $CO_2$ reduction and $H_2$ evolution on transition-metal electrocatalysts. *ACS Catal* 2014;4:3742-8. DOI
74. Chang X, Wang T, Gong J. $CO_2$ photo-reduction: insights into $CO_2$ activation and reaction on surfaces of photocatalysts. *Energy Environ Sci* 2016;9:2177-96. DOI

75. Chen S, Yuan H, Morozov SI, et al. Design of a graphene nitrene two-dimensional catalyst heterostructure providing a well-defined site accommodating one to three metals, with application to $CO_2$ reduction electrocatalysis for the two-metal case. *J Phys Chem Lett* 2020;11:2541-9. DOI
76. Breiman L. Random forests. *Mach Learn* 2001;45:5-32. DOI
77. Jiang Z, Zhou W, Hu C, et al. Interlayer-confined nife dual atoms within $MoS_2$ electrocatalyst for ultra-efficient acidic overall water splitting (Adv. Mater. 32/2023). *Adv Mater* 2023;35:2370227. DOI
78. Zhao Z, Lu G. Computational screening of near-surface alloys for $CO_2$ electroreduction. *ACS Catal* 2018;8:3885-94. DOI
79. Li H, Reuter K. Active-site computational screening: role of structural and compositional diversity for the electrochemical $CO_2$ reduction at Mo carbide catalysts. *ACS Catal* 2020;10:11814-21. DOI
80. Kour G, Mao X, Du A. Computational screening of single-atom alloys TM@Ru(0001) for enhanced electrochemical nitrogen reduction reaction. *J Mater Chem A* 2022;10:6204-15. DOI
81. Liu S, Xing G, Liu J. Computational screening of single-atom catalysts for direct electrochemical $NH_3$ synthesis from NO on defective boron phosphide monolayer. *Appl Surf Sci* 2023;611:155764. DOI
82. Chen Z, Zhao J, Cabrera CR, Chen Z. Computational screening of efficient single-atom catalysts based on graphitic carbon nitride (g-$C_3N_4$) for nitrogen electroreduction. *Small Methods* 2019;3:1800368. DOI
83. Zhao Z, Chen Z, Lu G. Computational discovery of nickel-based catalysts for $CO_2$ reduction to formic acid. *J Phys Chem C* 2017;121:20865-70. DOI